Phase Behavior and Microstructure of Poly(oxyethylene)−Poly(dimethylsiloxane) Copolymer Melt

Md. Hemayet Uddin,[†] Carlos Rodriguez,[†] Arturo López-Quintela,[‡] Dietrich Leisner,[§] Conxita Solans,[⊥] Jordi Esquena,[⊥] and Hironobu Kunieda*,[†]

Graduate School of Environment and Information Sciences, Yokohama National University, Tokiwadai 79−7, Hodogaya-ku, Yokohama 240-8501, Japan, Departamento de Química Física, Facultad de Química, Universidad de Santiago de Compostela, Santiago de Compostela, Spain, Research Center for Materials Science, Nagoya University, Chikusa, Nagoya 464-8602, Japan, and Departament de Tecnologia de Tensioactius, Institut d' Investigacions Quimiques i Ambientals de Barcelona, CSIC, Jordi Girona 18-26, 08034-Barcelona, Spain

Received July 12, 2002; Revised Manuscript Received December 2, 2002

ABSTRACT: Thermotropic phase behaviors of undiluted A−B type silicone copolymers, $Me_3SiO-(Me_2SiO)_{m-2}-Me_2SiCH_2CH_2CH_2-O-(CH_2CH_2O)_nH$ ($Si_mC_3EO_n$), have been studied as a function of both poly(dimethylsiloxane) chain length (m) and poly(oxyethylene) chain length (n). Differential scanning calorimetry, small-angle X-ray scattering, and video enhanced microscopy have been employed to construct phase diagrams and characterize microstructures. Three distinct ordered-state morphologies were observed for the $Si_{25}C_3EO_n$ system: micellar cubic (I_2), hexagonal (H_2) (here, the subscript 2 indicates POE embedded in PDMS matrix), and lamellar (L_α), within the examined composition range $f = 0.06$ to 0.50 (f = volume fraction of the polyoxyethylene part). Only H_2 and L_α ordered phases were observed in the studied range $f = 0.33-0.80$ for the $Si_mC_3EO_{51.6}$ system. The I_2 phase is shown to have $Fd\bar{3}m$ or at least $Fd\bar{3}$ space group symmetry. The effective cross-sectional area per copolymer molecule at the A−B interface, a_P, increases with increasing both m and n, while the morphologies change in the direction from L_α to H_2 with m and I_2 to H_2 to L_α with n. The compositional range for the formation of the different microstructures in the absence of solvent is compared with that observed in the presence of solvents (water or silicone oil) and also with other copolymer melt systems.

I. Introduction

A−B type linear block copolymers are of special interest in both theoretical and experimental studies, since they have a simple structure consisting of two chemically distinct incompatible blocks. The copolymers self-assemble into different ordered morphologies through block segregation, such as cubic lattice of spheres, hexagonally packed cylinders, and flat lamellae and also bicontinuous structures.[1−3] The distinguishable physicochemical and mechanical properties of these structurally well-defined morphologies lead to important technological applications.[4] Several theoretical studies predict symmetric phase behavior for a conformationally symmetric A−B block copolymer melt in a χN vs f phase diagram, where f is the volume fraction of A in the copolymer, χ is the Flory−Huggins interaction parameter between the segments A−B, and N is the overall polymerization degree.[5,6] The product χN is related to M_w/T since N is proportional to the copolymer molecular weight (M_w) and χ is $\sim 1/T$ (K^{-1}). This product expresses the degree of segregation. A decrease of the temperature or an increase in the copolymer size increases the degree of segregation and hence increases the stability of the ordered morphologies. f is a composition variable which can be varied by either synthesizing individual block copolymers or by mixing two different sized block copolymers. This parameter primarily dictates the interfacial curvature, the kind of micromorphology, and the ordered state symmetry.

There have been reports on experimentally determined phase diagrams for one-component block copolymer systems.[7] Experimental results however qualitatively differ from the theoretical predictions, mainly because of chain fluctuations and the conformational asymmetry of the blocks.[8] Low molecular weight amphiphiles, namely poly(oxyethylene) type nonionic surfactants (C_mEO_n), also self-organize in different ordered structures, and the morphologies change with changing the water and/or oil content, the hydrophile-lipophile balance of the surfactant and the temperature.[9−11] Poly(oxyethylene)−poly(ethylethylene) (POE−PEE) diblock copolymers are structural analogues of C_mEO_n surfactants. The POE−PEE block copolymers in the melt form ordered microstructures at low molecular weight and have been used as models for understanding surfactant phase behavior.[12,13] The phase behavior and microstructures for POE−poly(oxybutylene) have been studied by Mai et al. at low molecular weight (2−10 kDa).[14] Alexandridis[15] has reviewed POE-based copolymers and studied POE−poly(oxypropylene) (POE−POP) in selective solvents. The POE−POP copolymer mostly does not undergo microphase separation in the absence of solvent, due to the low tendency of block segregation.

Poly(oxyethylene)−poly(dimethylsiloxane) (POE−PDMS) diblock copolymers, consisting of incompatible and highly chemically different blocks, are of special interest for applications and fundamental research. The PDMS chain is very flexible and is a fluid even up to high molecular weights. Hence the molecular size of the copolymer can be varied from conventional surfactants to intermediate molecular weight copolymers.[16]

* Corresponding author. Telephone and fax: +81-45-339-4190. E-mail: kunieda@ynu.ac.jp.
[†] Yokohama National University.
[‡] Universidad de Santiago de Compostela.
[§] Nagoya University.
[⊥] Institut d' Investigacions Quimiques i Ambientals de Barcelona, CSIC.

10.1021/ma0210978 CCC: $25.00
Published on Web 01/30/2003

The A−B type silicone copolymer or surfactant forms almost all classical ordered microstructures, such as normal (PDMS in POE) and reverse (POE in PDMS) cubic (I_1, I_2), normal and reverse hexagonal (H_1 and H_2) and lamellar (L_α) phases in water[17] and L_α, H_2, and I_2 phases in nonpolar oils, such as low molecular weight silicone oil and hydrocarbon oils.[18] During the construction of these phase diagrams in the presence of solvents, we observed that the silicone copolymers can also form ordered morphologies in the bulk state. For example, silicone copolymer or surfactant with molecular weight $M_w = 1622$, $N = 26$ and $f = 0.29$ forms a H_2 phase in a narrow range of temperatures.[18,19] The ordered structures are not unexpected for such copolymers despite the low molecular weight of their blocks, because of the high incompatibility of POE and PDMS which can be deduced from their solubility parameters of 9.5 and 6.4 $(cal/cm^3)^{1/2}$, respectively.[20] Although Almdal et al.[21] studied the melt phase behavior of hydrocarbon-PDMS diblock copolymers, there are no systematic studies on the phase behavior of POE−PDMS copolymer melt.

Within the mean field theory for diblock copolymers, Matsen and Bates[6] predicted the existence of a body-centered cubic (bcc, Q^{229}) phase, at low and high f values, between the cylindrical and the disordered phases, and most of the experimental results seem to agree with that. In addition to this, these authors predicted also a second spherical phase where the spheres are arranged in a closed-packed lattice, in a very narrow region along the order−disorder transition for $\chi N \geq 18$. We reported for the first time the $Fd\bar{3}m$ (Q^{227}) cubic symmetry (at $f = 0.24$) in a bulk silicone copolymer.[22] However, this structure was previously found in binary lipid−[23] and copolymer−solvent[24] systems.

In the present study, we report the thermotropic phase behavior of two series of POE−PDMS diblock copolymers for constant PDMS chains and varying POE, as well as for constant POE and varying PDMS, with the polyoxyethylene volume fraction in the range $f = 0.06-0.80$. Not only will the results enrich the experimental data for copolymer melt phase behaviors using a new copolymer in relatively low molecular weight range (2−6 kg/mol), but also they can be used as an useful guide for new theoretical studies about the possible existence of an equilibrium $Fd\bar{3}m$ cubic morphology in copolymer melts.

II. Experimental Section

A. Materials. Poly(oxyethylene)−poly(dimethylsiloxane) diblock copolymers with the general formula $Me_3SiO-(Me_2SiO)_{m-2}-Me_2SiCH_2CH_2CH_2-O-(CH_2CH_2O)_nH$ ($Si_mC_3EO_n$) were obtained from Dow Corning Toray Silicone Co. Ltd., Japan. Me denotes a methyl group attached to Si, m is the total number of silicone units, and n is the average number of ethylene oxide (EO) units. The volume fraction of $CH_2CH_2CH_2$ in the copolymer is only ~2% or less and it is compatible with the PDMS block at the investigated temperatures; therefore we consider the copolymer as an AB-type block copolymer instead of an ABC triblock copolymer. The silicone polyether was prepared by a sequential anionic polymerization as described elsewhere.[18] Table 1 shows data corresponding to the copolymers as received. The polydispersity indices, M_w/M_n of poly(oxyethylene) and poly(dimethylsiloxane) blocks of copolymers were measured by gel permeation chromatography. The main impurity is unreacted polyether except $Si_{25}C_3EO_{51.6}$ which contains unreacted poly(dimethylsiloxane). The silicone oil was removed by washing the copolymer with hexane at least three times. Water content was measured by the Karl Fischer method with a Mitsubishi CA-06 moisturemeter. The copolymers were treated by washing with methanol to remove water and unreacted polyether and, after evaporation of the solvent by using vacuum evaporator, dried over P_2O_5.

Table 1. Data for $Si_mC_3EO_n$ Copolymers as Received

m	n	purity (wt %)[a]	PI_m[b]	PI_n[b]	water (wt %)	M_p[c]	f_{E0}
25	3.2	97.9	1.20	1.21	0.105	2053	0.06
25	7.8	96.2	1.20	1.26	0.223	2256	0.14
25	12.2	93.7	1.20	1.16	0.537	2449	0.20
25	15.8	93.1	1.20	1.20	1.010	2608	0.24
5.8	51.6	99	1.02	1.13	0.578	2761	0.80
14	51.6		1.19	1.13	0.666	3369	0.64
25	51.6	94.6	1.20	1.13	0.337	4185	0.50
38	51.6		1.06	1.13	0.129	5149	0.40
52	51.6		1.07	1.13	0.059	6187	0.33

[a] Excluding water content. [b] PI_m and PI_n stand for the polydispersity index of poly(dimethylsiloxane) and poly(oxyethylene) chains, respectively. $PI = M_w/M_n$, where M_w is the weight-average molecular weight and M_n is the number-average molecular weight. [c] M_P is the average molecular weight of the copolymer.

B. Determination of Phase Diagrams. Each homogeneous copolymer was sealed in glass ampules. Intermediate samples were prepared by weighing various amounts of two neighboring different POE or PDMS chain length copolymers in ampules. The ampules were flame-sealed immediately. The molten copolymer constituents were mixed using a vortex mixture and homogeneity was attained by repeated centrifugation through a narrow constriction in the sample tubes. The phase equilibrium was investigated by visual inspection of the samples in normal light and between crossed polarizers to detect optically anisotropic phases, e.g. the lamellar and the hexagonal phases. Solid−ordered phase transition temperatures were also measured by differential scanning calorimetry. The structures of ordered phases were identified by means of video-enhanced microscopy (VEM) and small-angle X-ray scattering (SAXS) measurements.

C. Optical Microscopy. A differential interference phase-contrast microscope (Nikon, ×2F−NTF-21) equipped with a video enhanced system (Sony, 3CCD Exwave HAD) was used to observe anisotropic phases. The samples were placed between a clean, dust free slide (76 × 26 × 1 mm) and a cover glass (18 × 18 × 1 mm) on a temperature controlled hot stage Mettler FP82 for the measurements.

D. Small-Angle X-ray Scattering (SAXS). SAXS measurements on viscous isotropic samples (cubic phase) were performed on a small-angle scattering goniometer with an 18 kW Rigaku Denki rotating anode generator (Rint-2500) operating at about 25 °C. The cubic samples were equilibrated for several weeks in a thermostatic water bath. At elevated temperatures, measurements were performed in a Mbraun instrument equipped with a Siemens K-760 generator, operating at 50 kV and 20 or 30 mA, and a Kratky Heccus Mbraun-Graz camera. The collimator was a slit window and the detector an OEM-50M. The temperature controller was an AP Paar K-PR (25−300 °C). Samples measured at 53 and 58 °C were equilibrated for a minimum of 2 days in thermostated water baths. Viscous samples were placed in cells of Mylar film. Less viscous samples were placed in glass capillaries of 1 mm diameter and 10 μm wall thickness. Smearing was corrected in all measurements according to the method described in ref 25. Scattering of samples placed in capillaries was measured in absolute scale subtracting scattering produced by the glass capillary.

The structure of the cubic phase in the present copolymer system is difficult to determine due to the soft micelles (with very flexible poly(dimethylsiloxane) coronae) present and due to the long equilibration time. In the in-house measurements, the number of resolved reflections is too scarce as to assign them to a certain space group. Therefore, a sample in the cubic region was measured at different temperatures by using the synchrotron radiation SAXS spectrometer of the BL-10C instrument installed at the Photon Factory (PF), High Energy Physics Research Institute (KEK), Tsukuba, Japan. The

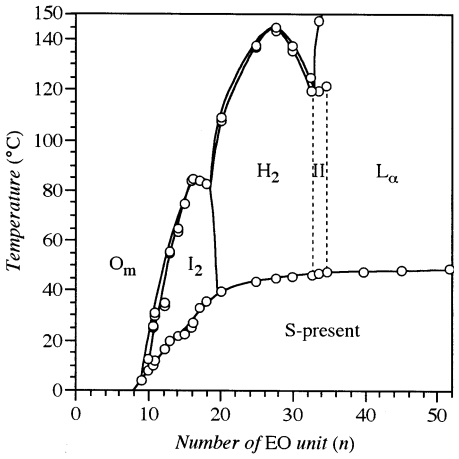

Figure 1. Phase diagram of the $Si_{25}C_3EO_n$ system as a function of the poly(oxyethylene) chain length, n. I_2, H_2, and L_α represent discontinuous micellar cubic, hexagonal, and lamellar phases, respectively, and O_m represents the (POE in PDMS) micellar or copolymer liquid phase. II is a two-phase region. S represents the solid component.

scattered X-ray was detected using a position sensitive proportional counter. A copper-made sample cell with Kapton windows was used, and the temperature of the sample was controlled within a precision of 0.01 K.

A similar sample was measured between Kapton films in a thermostated cell-holder, placed in a 50 mm wide air gap of a Rigaku 3-slit pinhole camera equipped with Osmic confocal multilayer optics for Cu Kα and a Fuji IP 2D-detector, at 1000 mm sample−detector distance. Azimuthally averaged scattering patterns from never spotty diffractograms were background corrected but not desmeared, although the beam divergence was considerable (fwhm = 0.034 nm^{-1}).

III. Results

A. Thermotropic Phase Behavior: $Si_{25}C_3EO_n$ System. The thermotropic phase behavior of undiluted (bulk) poly(oxyethylene)−poly(dimethylsiloxane) copolymers ($Si_{25}C_3EO_n$) as a function of POE chain length (n, ranging from 3.2 to 51.6 when f ranges from 0.06 to 0.50) is presented in Figure 1. Five different POE chain copolymers: $Si_{25}C_3EO_{3.2}$, $Si_{25}C_3EO_{7.8}$, $Si_{25}C_3EO_{12.2}$, $Si_{25}C_3EO_{15.8}$, and $Si_{25}C_3EO_{51.6}$ were used to construct the phase diagram. The intermediate samples were prepared by mixing two neighboring POE chain copolymers. At room temperature, $Si_{25}C_3EO_n$ are isotropic liquids up to $n \approx 10$, and for $n > 10$ the copolymers form either ordered phases or solids. The melting temperature of the solid phase (T_m) was measured visually and also by DSC. With the increase of POE chain length the T_m increases steeply up to $n = 20$, whereas for $n > 20$ the increase is less pronounced. The T_m values of the copolymers mainly depend on the chain length of the semicrystalline polyoxyethylene since poly(dimethylsiloxane) is in a liquid (or amorphous) state up to high molecular weights.[16] The increase in T_m with the molecular mass, for low-molecular-mass polymers, is a well-known phenomenon in polymers[26] and is due to the decrease of the number of chain ends (and therefore defects) inside a crystal domain.

Above the melting temperature of the solid phase, $Si_{25}C_3EO_n$ forms a liquid containing copolymer micelles (with POE core and PDMS corona), O_m, as well as different ordered morphologies. The ordered phases include micellar cubic (I_2), hexagonal (H_2) and lamellar (L_α) phases. Here, the subscript 2 indicates that the polar POE chain is embedded in the apolar PDMS matrix. The thermal stability of the ordered phases increases with increasing POE chain length and hence with the increase of the copolymer molecular weight. The isotropic O_m and I_2 phases are easily detected since the viscosity of the I_2 phase is significantly higher than that of the O_m phase. The H_2 and L_α phases are also waxy and were identified by their typical video-enhanced microscope textures. The characteristic VEM pictures for the H_2 and L_α phases are shown in Figure 2. There is a two-phase region (II) between the H_2 and L_α phases. This $H_2 + L_\alpha$ mixture appears turbid and birefringent, and flows with the gravitational force at comparatively lower temperatures than either the homogeneous H_2 or the L_α phases. The two-phase coexistence is only observed in the blend of two block copolymers ($Si_{25}C_3EO_{15.8}$ and $Si_{25}C_3EO_{51.6}$) with very different relative block sizes and thus is not a violation of the Gibbs phase rule.

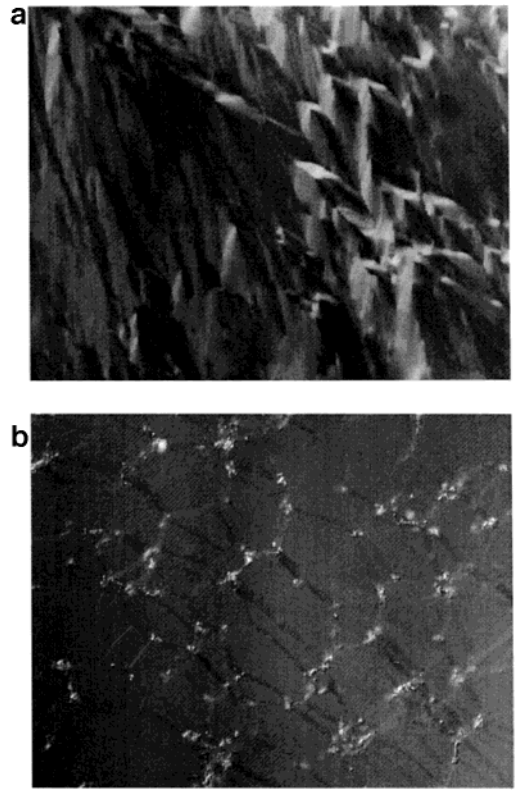

Figure 2. Typical optical microscope (VEM) textures: (a) $Si_{25}C_3EO_{25}$, H_2 phase at 80 °C (b) $Si_{25}C_3EO_{51.6}$, L_α phase at 95 °C.

$Si_mC_3EO_{51.6}$ System. Phase behavior of dry poly(oxyethylene)−poly(dimethylsiloxane) copolymers ($Si_mC_3EO_{51.6}$) as a function of Si chain length (m, ranges from 5.8 to 52 when f ranges from 0.80 to 0.33) is presented in Figure 3. Five copolymers with different Si chain lengths, $Si_{5.8}C_3EO_{51.6}$, $Si_{14}C_3EO_{51.6}$, $Si_{25}C_3EO_{51.6}$, $Si_{38}C_3EO_{51.6}$, and $Si_{52}C_3EO_{51.6}$, were used to construct the phase diagram. The intermediate samples were prepared by blending two neighboring Si chain copolymers. At room temperatures the samples look white powderlike for short Si chain and bluish waxylike for long Si chain copolymers. The copolymers melt to either anisotropic phases or fluid isotropic phases at ∼ 50 °C. I and II indicate the isotropic liquid phases in the transparent and turbid regions, respectively. The copolymer $Si_{5.8}C_3EO_{51.6}$, represented by the dotted line in Figure 3, is an almost transparent and optically isotropic fluid above the melting temperature. However, upon adding a small

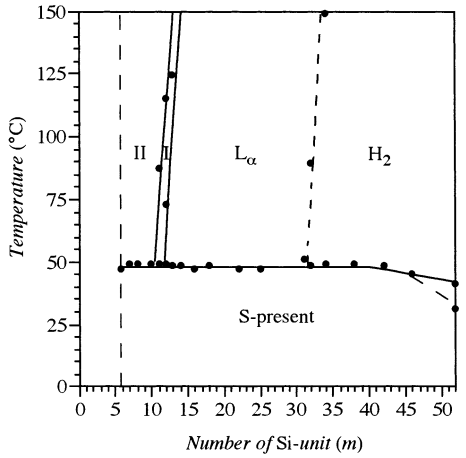

Figure 3. Phase diagram of the $Si_mC_3EO_{51.6}$ system as a function of the poly(dimethylsiloxane) chain length, m. H_2 and L_α represent reverse hexagonal and lamellar phases, respectively, and I represents the (PDMS in POE) micellar or copolymer liquid phase. II represents immiscible copolymer liquids. The dotted line indicates the sample $Si_{5.8}C_3EO_{51.6}$; measurements have not been performed for $m < 5.8$. S represents a solid.

amount of $Si_{14}C_3EO_{51.6}$, the samples become turbid; that is, there is a large miscibility gap between two copolymers (region II). Beyond region II, the two copolymers $Si_{5.8}C_3EO_{51.6}$ and $Si_{14}C_3EO_{51.6}$ mix well with each other, and an isotropic transparent liquid phase, probably a normal micellar phase, is observed (I). Ordered anisotropic phases, L_α and H_2, are observed for $m > 12$ in the phase diagram and were distinguished by their typical VEM textures and the SAXS peak ratios. In both regions, the samples are completely transparent and strongly birefringent. Concerning the viscosity, the samples in the H_2 phase are more viscous than in the L_α phase. The H_2 and L_α phases are thermally stable up to at least 150 °C, except in the vicinity of the phase boundaries, where the L_α−I (isotropic solution) and the H_2−L_α first-order phase transitions occur. With the increase in PDMS length, for a constant POE chain, a bilayer in the L_α phase is changed to a cylinder with a POE core and a PDMS corona.

B. Microstructure. The different microstructures observed for the $Si_{25}C_3EO_n$ and $Si_mC_3EO_{51.6}$ systems were determined from the relative Bragg peak positions. Parts a−c of Figure 4 represent the schematics of the I_2, H_2, and L_α structures and their structural parameters, respectively. The interlayer spacings, d, of different phases were obtained from the first-order SAXS reflection peaks. To calculate the interfacial area per amphiphilic molecule, a_P, in different phases we assumed that the microstructures consist of two components, namely polar (POE) and apolar (PDMS + $(CH_2)_3$) domains, separated by a sharp interface. The volume fraction of the poly(oxyethylene) part of copolymers, $f = V_{EO}/V_P$, was calculated from the molar volumes of poly(oxyethylene) (V_{EO}) and copolymer (V_P).[17] The volume fraction of the apolar part f_{apolar} is $(1 - f)$.

The Reverse (POE Core) Micellar Phase, O_m. $Si_{25}C_3EO_n$ with $n < 7.8$ has liquid like structure (disordered); with $n \geq 7.8$ POE minority micelles are formed (Figure 1) as can be understood from the broad correlation peaks represented in Figure 5. A flat diffraction pattern is observed for $Si_{25}C_3EO_{3.2}$, indicating that no aggregates are formed for such a short EO chain copolymer. When the EO chain is very short, the

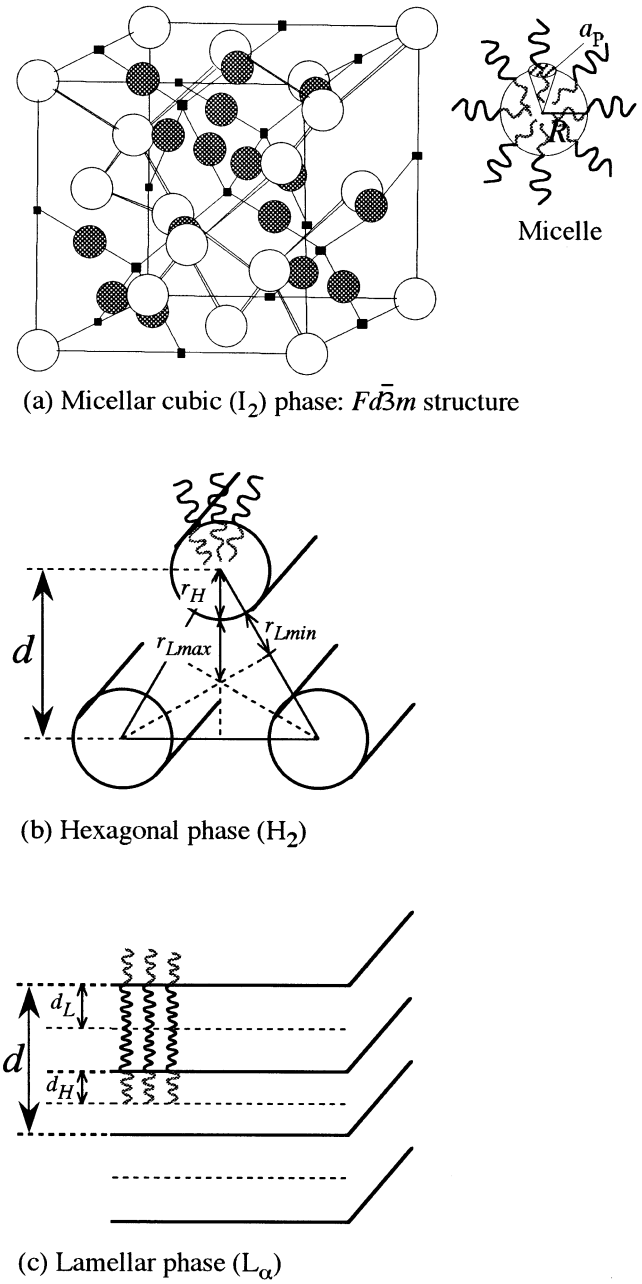

Figure 4. (a) Schematic representation of the I_2 phase ($Fd\bar{3}m$ space group). The unit cell contains 8 micelles of symmetry $43m$ (white) and 16 micelles of symmetry $\bar{3}m$ (shaded). The lines are only a guide to the eye. Adapted from ref 31. Schematic representations of the H_2 phase (b) and the L_α phase (c).

segregation between the two blocks is too weak for micelle formation. $Si_{25}C_3EO_{3.2}$ does not even aggregate in solvents such as octamethylcyclotetrasiloxane (D_4) or decane. However, $Si_{25}C_3EO_{7.8}$, $Si_{25}C_3EO_{12.2}$ and $Si_{25}C_3EO_{15.8}$ form micelles in these solvents.[18] $Si_{25}C_3EO_{7.8}$ shows a very broad peak at $q_{max} = 0.22$ nm^{-1}, whereas $Si_{25}C_3EO_9$ shows a comparatively strong correlation peak at $q_{max} = 0.35$ nm^{-1}. The peak position q_{max} depends on both the micellar volume fraction, ϕ, and the hard-sphere interaction distance, r_{HS}, if micelles are considered as hard spheres. As was previously found[27] in block copolymer systems, despite the disperse polymer corona, a near-hard sphere interaction potential is expected as a result of the entropic repulsion. The scattering intensity can then be estimated assuming a form factor of a dense spherical object with a sharp

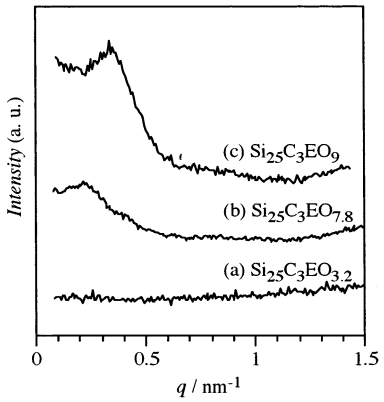

Figure 5. SAXS diffraction patterns obtained from $Si_{25}C_3EO_n$ at 25 °C. (a) $Si_{25}C_3EO_{3.2}$ gives a flat pattern indicating no aggregate formation. (b) $Si_{25}C_3EO_{7.8}$ and (c) $Si_{25}C_3EO_{15.8}$ show wide correlation peaks indicating formation of aggregates.

interface of radius r_c and a structure factor determined by the Ornstein−Zernike and Perkus−Yevick approximations[28] using a hard-sphere interaction potential. From the fitting of the diffraction patterns, r_c, r_{HS}, and ϕ can be obtained. The values obtained are as follows: for $Si_{25}C_3EO_{7.8}$, $r_c = 5.9$ nm, $r_{HS} = 1.3\ r_c$, and $\phi = 0.08$, whereas for $Si_{25}C_3EO_9$, $r_c = 6.2$ nm, $r_{HS} = 1.05\ r_c$, and $\phi = 0.20$. The r_c values obtained agree with those calculated from the extrapolated data of the micellar core radius obtained in the cubic phase (see later, Figure 12a) and the effective length of the siloxane chain ($l_{eff} \approx 2.7$ nm): r_c ($Si_{25}C_3EO_{7.8}$) = 5.5 nm; r_c ($Si_{25}C_3EO_9$) = 5.8 nm. It is interesting to note that the increase of the repulsive interactions when the POE chain length increases leads to an increase of the micellar volume fraction ($\phi = 0$, 0.08, 0.20, 1 for $n = 3.2$, 7.8, 9, and 10, see below, respectively) which shows the increase of the segregation between the copolymer blocks.

The Micellar Cubic Phase, I_2. For higher POE block lengths, the micelles crystallize into a cubic lattice. The I_2 phase exists between the O_m and the H_2 phases from $n = 10-20$, as can be seen in Figure 1. The samples in this region are quite transparent, nonbirefringent, and very stiff. The cubic phase shows diffraction patterns with diffraction peaks, demonstrating long-range order. Figure 6a represents the SAXS diffraction patterns performed at temperatures 30, 50, and 70 °C for a bulk $Si_{25}C_3EO_{15.8}$ sample forming the cubic phase at temperatures between 23 and 85 °C. The diffraction patterns show almost the same peak positions (indicated by dotted lines) and the same peak heights for the [311] peak, the most intense one at different temperatures. The [311] peak position at 30 °C is slightly shifted to lower q values. Because of the thermal annealing an increase of the domain size with temperature can be expected. Then, at low temperatures wider peaks corresponding to smaller domain sizes are obtained. In this case, an overlapping of neighbored Bragg peaks, with an apparent shift in the peak positions, may occur, as it is observed with the [220] and [311] reflections. On the other hand, at high temperatures, the total number of resolved peaks increases and the higher order peaks become increasingly intense because of the increase of the domain size with temperature. A maximum of 13 Bragg peaks were identified at 70 °C, which can be indexed as the [111, 220, 311, (222), 400, 331, (422), 511/333, 440, 442, 620, 533] and [444] reflections of a cubic aspect 15, namely, $Fd\bar{3}m$ (Q^{227}) and $Fd\bar{3}$ (Q^{203}).[23] All permitted reflections below [444] are observed, except

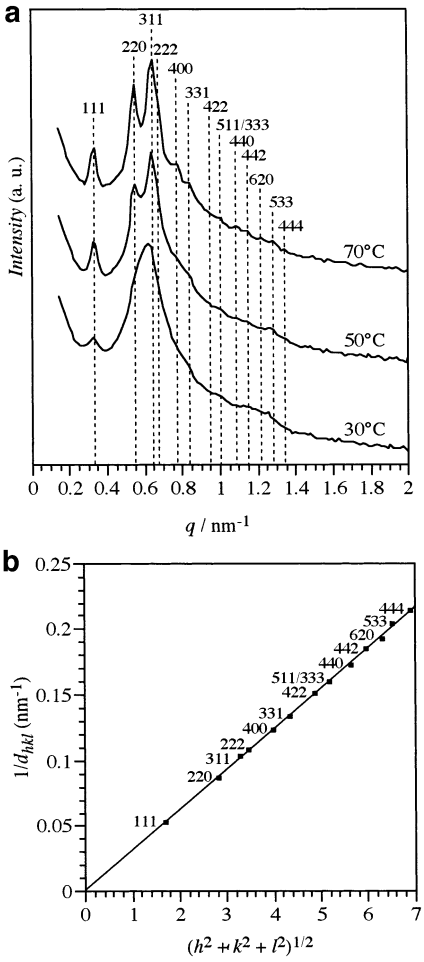

Figure 6. SAXS data obtained from $Si_{25}C_3EO_{15.8}$. (a) Diffraction pattern as a function of the scattering vector amplitude, q, at 30, 50, and 70 °C. Dotted lines indicate reflections corresponding to the $Fd\bar{3}m$ space group. (b) Plot of the reciprocal d spacings ($1/d_{hkl}$) of the reflections obtained at 70 °C marked in part a, vs $(h^2 + k^2 + l^2)^{1/2}$.

those from [531] and [622]. Some of the reflections, such as [222] (not pronounced), [531] and [622] are most likely covered by the strong [311], [442], and [533] reflections, respectively. In accordance with the suggestion of Luzzati and co-workers, we assume that the more symmetrical space group, $Fd\bar{3}m$ (Q^{227}), is the correct one.[29] The lattice parameter (the cubic unit cell length), of a cubic structure is given by $a = 2\pi\sqrt{h^2 + k^2 + l^2}/q_{hkl}$ where q_{hkl} is the scattering vector amplitude of the [hkl] reflection and h, k, and l are the Miller indices. The plot of the reciprocal d spacings ($1/d_{hkl} = q_{hkl}/2\pi$) vs $(h^2 + k^2 + l^2)^{1/2}$ fits a straight line (Figure 6b) passing through the origin, in agreement with the cubic aspect 15 ($Fd\bar{3}m$ or $Fd\bar{3}$ space group). The lattice parameter, obtained from the reciprocal slope of the plot, is 32.3 nm. This value showed almost no variation (32.2−32.5 nm) in a temperature scan from 30 to 70 °C.

The $Fd\bar{3}m$ space group mostly has been found for the reverse type cubic (I_2) phase in some binary[23] and ternary[24] surfactant or copolymer lyotropic systems. Since the SAXS pattern obtained is similar to those $Fd\bar{3}m$ cubic phases, it is quite possible that this phase has the structure proposed by Charvolin and Sadoc[30] and later confirmed by Luzzati et al.[31]

Cubic Structure of the $Si_{25}C_3EO_{15.8}$ Phase at 70 °C. Although we have assigned the possible cubic

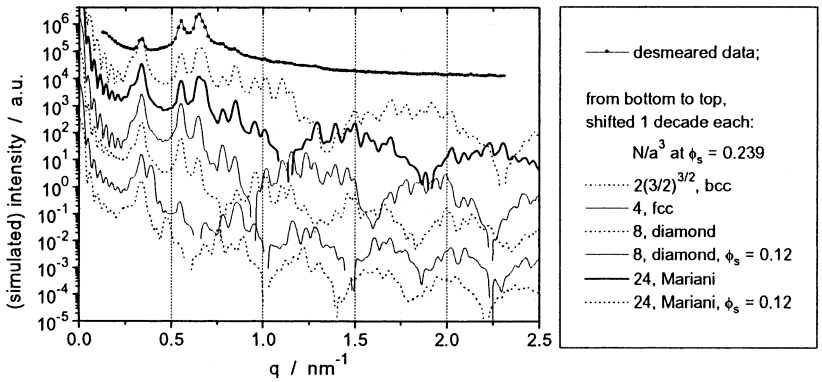

Figure 7. Comparison of desmeared SAXS data with calculated scattering curves for micelles with a homogeneous core and a corona of Gaussian chains, assembled into different ideal cubic crystals of 6^3 unit cells with $a = 32.2$ nm, $\phi_S = 0.239$ and $R_B = 1.314$ nm. Only the F_S and F_{SC} contributions have been modulated with the cubic lattice structure factors from Figure 2. The core radius R, the aggregation number N_C, and ρ_C/ρ_S are given by ϕ_S (see text).

structure is $Fd\bar{3}m$, the micelles in diblock copolymer melts are usually expected to crystallize either in bcc (Q^{229}), fcc (Q^{225}), or hcp (Q^{194}) lattices.[32] For further discussion, we represent the calculated scattering functions (discussed below) for different lattices together with the experimental azimuthal averaged and desmeared excess synchroton−SAXS intensity for the cubic I_2 phase of $Si_{25}C_3EO_{15.8}$ at 70 °C, obtained after appropriate annealing time in Figure 7. The weakness of high-order reflections observed in the scattering patterns is commonly due to natural lattice imperfections and limited domain size, the nonobservation of low-order Bragg reflections besides observed higher-order reflections must be due to specific extinctions, that is, to minima in the form factor of the "objects" centered in the nodes of the lattice or to improper powder-averaging as a result of a too small number of grains in the scattering volume of a static nonergodic sample.

For a comparison of the scattering pattern with the expected ones for these lattices, one which allows even to judge the proper amplitude ratios of the Bragg peaks, the structure factors $S(q)$ for ideal lattices composed of $n \times n \times n$ unit cells were calculated, with lattice constants a that would give the first-order Bragg reflection at the same q as the first experimentally observed Bragg peak. The calculation was performed applying the Wierl equation

$$S(q) = \frac{1}{N_m{}^2} \sum_{i=1}^{N_m} \sum_{j \neq i}^{N_m} \frac{b_i b_j}{\langle |b| \rangle^2} \frac{\sin(qr_{ij})}{qr_{ij}} \qquad (1)$$

where the b_i, b_j are the (excess) scattering lengths in nodes i and j of the considered lattice, respectively, $\langle |b| \rangle$ is the ensemble averaged (absolute excess) scattering length per node, and r_{ij} is the distance between nodes i and j. The values of $S(q)$ are plotted in Figure 8 for comparison. From the relative positions of the principal peaks, hcp and bcc structures could, in principle, be ruled out. The fcc (Q^{225}) structure could match the experimental data, if one could find arguments for the selective suppression of the [200] reflections. We will come back to this point later on.

Now we will examine other different assemblies of copolymer micelles on a $Fd\bar{3}m$ lattice, namely, the diamond structure. A diamond structure could be built if one puts the constraint that monodisperse hard spheres will be packed as close as possible in that symmetry: eight hard spheres of radius $R_8 = a \times 3^{1/2}/8$

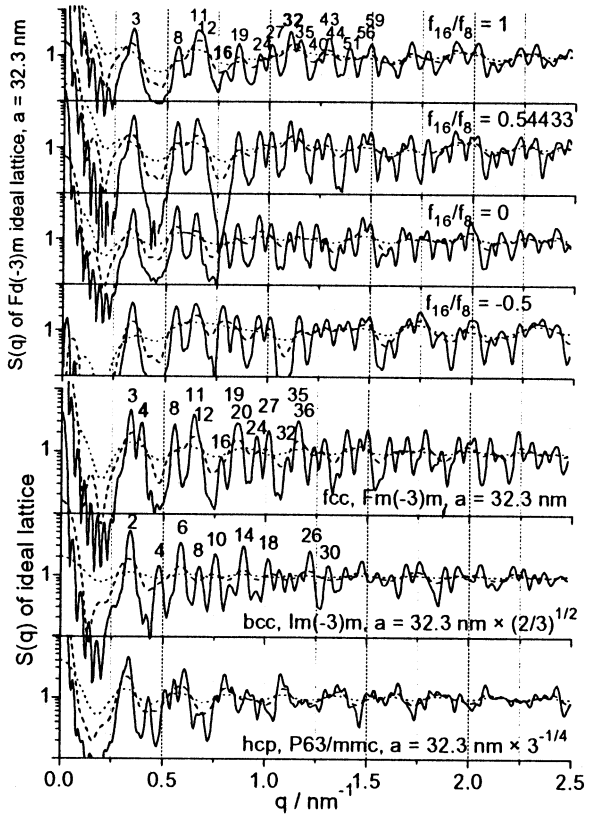

Figure 8. Lattice structure factors calculated by eq 1 (Wierl equation) for stacks of 1 (dotted), 2^3 (dashed), and 6^3 (solid lines) ideal unit cells with lattice constant $a = 32.3$ nm. For hcp, a refers to the closest distance between nodes. f_{16}, f_8 refer to the scattering lengths in the 8 diamond and additional 16 lattice nodes of Mariani's proposed I_2 structure.[23,33] Numbers above reflections denote the $(h^2 + k^2 + l^2)$.

per unit cell (on Wyckoff position 8*a*) yielding a filling factor 0.34. For micelles with variable aggregation number N_c, multimodal size distributions could be achieved if the energy for the deviation from the ideal size is compensated by a better packing. The largest gaps in the previous structure can be filled with 16 smaller hard spheres of radius $R_{16} = a \times 2^{1/2}/8$ (on Wyckoff position 16*c*), which would touch along diagonal channels and in tetrahedra. This structure has been proposed by Mariani et al.[29,33] for another I_2 phase. The minimum distance between hard spheres of different size is $d_{8-16,min} = a \times 11^{1/2}/8$. The ratio of the volumes occupied by the individual closest-packed hard spheres

is $V_{16}/V_8 = (2/3)^{3/2} \sim 0.544$, and the total filling factor is 0.71. If all hard spheres have the same scattering length density, then $b_i \propto V_i$, and the [400] reflection will be extinguished (see Figure 8). Our clear observation of the [400] reflection thus rules out this "bimodal close packing" for the studied case. We consider thus instead the possibility of packing the micelles with a monodisperse core radius R, distributed on the same 24 nodes as the bimodal hard spheres, but with asymmetric coronae. In this case, all the b_i are equal only if the segregation between copolymer blocks is complete and all the distortion is only in the softer corona. For the modeling, we will assume this to be the case.

We will discuss the possibility of a severe "attenuation" of one or more distinct Bragg reflexes of the possible structures by form factor minima. For the form factor calculation of the copolymer micelles, we apply the model of a hard sphere with radius R (representing the core which is formed by N_c POE blocks) and with N_c Gaussian chains attached (representing the corona)[34,35] with the parameter notation as in ref 34 (form factor $P_{25}(q)$, p 195). The core radius R must satisfy the number of micelles N_m per volume a^3 of the lattice, being $R = [3\phi_s/(4\pi N_m)]^{1/3}a$, where the core volume fraction is $\phi_s = f$. The aggregation number is $N_c = a^3/N_m/v_P$ with $v_P = 4.33$ nm^3 (volume per $Si_{25}C_3EO_{15.8}$ molecule). With the contour length $L_B = 6.7$ nm for the C_3−PDMS block, calculated from reported bond lengths and angles,[17,36] and considering the number of its Kuhn segments to be equal to the degree of polymerization (26, including one segment for the short C_3 middle block), we calculate the radius of gyration to be $R_B = (L_B^2/26)^{1/2} = 1.31$ nm. The ratio of the excess scattering length densities in the homogeneous matrix formed by the interpenetrating coronae of the micelles, ρ_c, to the one in the homogeneous spheres, ρ_s, of volume fraction ϕ_s, in this ideal case of complete segregation, is given by $\rho_c/\rho_s = -(\phi_s^{-1} - 1)^{-1}$, so that, with $\phi_s = f = 0.239$, we have $\rho_c/\rho_s = -0.314$.

We then calculate the scattering functions with the previous estimated parameters, being N_m lattice dependent. The F_s and F_c partial form factors for the contribution of the cores were modulated with the corresponding lattice structure factor $S(q)$ given in Figure 8, whereas the partial form factors F_c and F_{cc} for the correlations of the corona chains have not been modulated with $S(q)$, as their correlation with the lattice nodes is presumably marginal. The scattering functions are plotted in Figure 7 together with the experimental data for comparison.

Although the accuracy is restricted by the simplicity of the model, we see that the dominant hard sphere core form factor F_s produces its minimum for the large micelles in the bcc and fcc structures at $q \sim 0.6$ nm^{-1}, just where instead a scattering maximum is observed. Only if $\phi_s \ll f$, this means for a very incomplete segregation, the scattering could thus be consistent with the fcc (Q^{225}) structure. However, even in this case, the suppression of the [200] reflection cannot attributed to the form factor effect. The fcc structure can thus be ruled out.

Let us now finally examine the scattering from the different considered $Fd\bar{3}m$ structures. For the diamond structure ($N_m = 8$) and $\phi_s = f$, we would yet have micellar cores so large ($R = 6.2$ nm) that the form factor minimum is at $q \sim 0.75$ nm^{-1}, where instead still some weak Bragg reflexes can be observed. Only in the case of a very incomplete segregation, thus smaller cores (e.g., with $\phi_s = 0.12$, $R = 4.9$ nm), the diamond structure could fit the experimental data. With $N_m = 24$ micelles in the unit cell (Wyckoff position 16*c* also occupied), even at full segregation the core radii are so small ($R = 4.3$ nm) that the modeled form factor exhibits its first minimum at $q \sim 1.1$ nm^{-1}, a momentum transfer larger than all the observed Bragg reflections. Thus, even the form factor of the less hard-sphere-like real system cannot be expected to suppress any important Bragg reflection of that structure, which is consistent with the fact that all of them up to the [422] indexed have been observed. One remaining problem is the relatively low intensity of the observed first-order reflection ([111]). However, such a weak [111] reflection and a broad correlation peak underlying the [220] and [311] reflections has also been observed by Seddon et al.[23] The same feature is also observed in the scattering function for the phase obtained after melting the cubic phase at above 85 °C and quenching to 75 °C before starting a 22 h measurement (Figure 9c). It has qualitatively been reproduced by the calculated scattering of copolymer micelles interacting with a sticky hardsphere potential,[34,37] shown in Figure 9d.

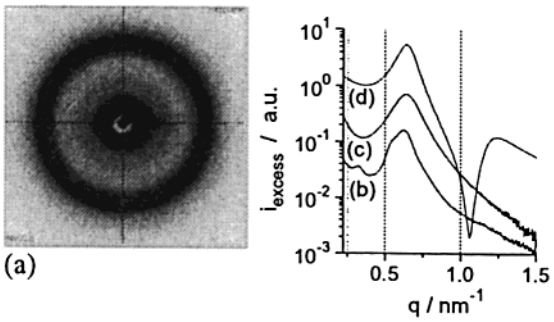

Figure 9. In-house SAXS 2-D scattering pattern (a), in the q_x and q_y range ±0.9 nm^{-1} with the attenuated direct beam imaged after removing the beam stop, and smeared azimuthally averaged and background corrected scattering curves (b, c) for $Si_{25}C_3EO_{15.8}$ 24 h annealed at 70 °C (a = b), and quenched to 75 °C after 1 h melting at 87 °C (c). Curve d is a simulated scattering function with the copolymer micelle form factor used before ($R = 4.3$ nm, $N_C = 321$), but with the F_S and F_{SC} modulated by a sticky hard sphere factor[34,37] with the sticky interaction radius $R_{HS} = 6$ nm, the fraction of the excluded volume $\eta = 0.52$, and the stickiness parameter $\tau = 0.45$.

Finally, the reproducibly smooth distribution of the azimuthal scattering intensity in the in-house SAXS experiments (Figure 9a) suggests that the grain number in the scattering volume was sufficient for a statistically correct powder pattern even in the synchroton SAXS experiment.

In conclusion we find that the cubic phase is almost certainly of $Fd\bar{3}m$ symmetry, and that the Mariani's proposed structure[23,33] in which the unit cell is filled with 24 micelles of equal core size per unit cell on Wyckoff 8*a* and 16*c* positions is the most probable. It has recently been shown by Monte Carlo simulations that star-polymers with a huge number of arms (>45) and with a spherically symmetric ultrasoft repulsive interaction potential would crystallize in a diamond lattice at high polymer packing density in the corona,[38] conditions that could well apply for our copolymer micelles with $N_c \geq 320$.

For simplicity and for comparison purposes hereafter, we assume that we have monodisperse spherical micelles ordered in a $Fd\bar{3}m$ structure. According to the

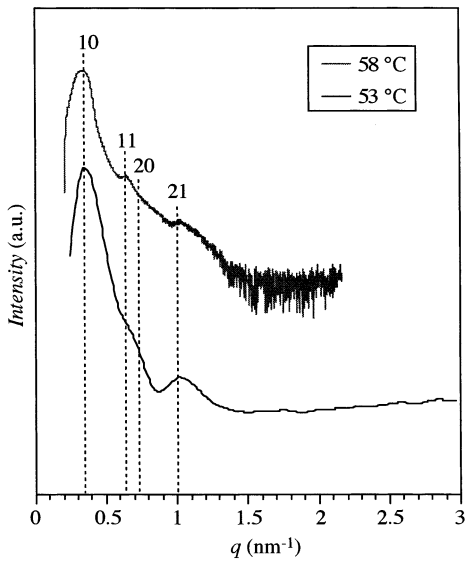

Figure 10. SAXS diffraction patterns of the H_2 phase in $Si_{52}C_3EO_{51.6}$ at 53 °C (azimuthal averaged and desmeared) (a) and 58 °C (smeared azimuthally averaged and background corrected) (b) scattering patterns.

geometry of the I_2 phase, the following equations can be derived for the calculation of the radius of the polar core of reverse micelles, R, and for the effective cross-sectional area per copolymer molecule, a_P,

$$R = C\left(\frac{3}{4\pi N_m} f\right)^{1/3} d \tag{2}$$

$$a_P = \frac{3v_P f}{R} \tag{3}$$

where d is the interlayer spacing measured by SAXS, $N_m = 24$ is the number of micelles per unit cell, and C is a constant ($C = (h^2 + k^2 + l^2)^{1/2}$). v_P is the volume of one copolymer molecule.

The Hexagonal Phase, H_2. The H_2 regions extend in the range of $n = 20-34$ for the $Si_{25}C_3EO_n$ system (Figure 1) and $m = 32-52$ for $Si_mC_3EO_{51.6}$ system (Figure 3). Representative SAXS diffraction patterns obtained from the H_2 phase ($Si_{52}C_3EO_{51.6}$, in Figure 3) at 53 and 58 °C are shown in Figure 10. The relative positions of the four observed Bragg peaks obey the $1:\sqrt{3}:2:\sqrt{7}$ relationship confirming the two-dimensional hexagonal structure. The radius r_H of the polar cylinder core, of volume fraction f, and the interfacial area per copolymer molecule, a_P, are given by

$$r_H = \left(\frac{2}{\sqrt{3}\pi} f\right)^{1/2} d \tag{4}$$

$$a_P = \frac{2v_P f}{r_H} \tag{5}$$

According to the geometry of the H_2 phase (Figure 4b), half of the longest distance between polar cores of two cylinders is

$$r_L = \frac{2d}{3} - r_H$$

The Lamellar Phase, L_α. The one-dimensional lamellar (smectic) structure (shown schematically in Figure 4c) applies to the samples in the L_α regions, $n =$ 36−51.6 for $Si_{25}C_3EO_n$ (Figure 1) and $m = 12-32$ for $Si_mC_3EO_{51.6}$ (Figure 3), as has been established by SAXS measurements that gave diffraction patterns in which the positions of the Bragg reflections obey the relationship 1:2:3. Figure 11 shows a representative SAXS diffraction pattern from the L_α phase ($Si_{25}C_3EO_{51.6}$, in Figure 1 or 3). The half-thickness of the polar domain d_H and the a_P in the L_α phase are given by

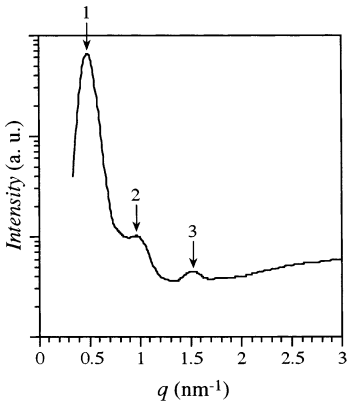

Figure 11. SAXS diffraction pattern of the L_α phase in $Si_{25}C_3EO_{51.6}$ at 53 °C.

$$d_H = \frac{fd}{2} \tag{6}$$

$$a_P = \frac{v_P f}{d_H} = \frac{2v_P}{d} \tag{7}$$

The half-thickness of the apolar domain is $d_L = (1 - f)d/2$.

C. Variation in the Characteristic Structural Parameters and Phase Transitions: $Si_{25}C_3EO_n$ System. The interlayer spacing corresponding to the [311] Bragg reflection (the most intense one in Figure 6a) of the I_2 phase was measured by SAXS. The variation of d, R, and a_P as a function of POE chain length (n) is shown in Figure 12a at 25 °C. With the increase of n or f the polar core of micelles grows and consequently d and R increase. a_p also increases with increasing n because of increasing repulsion between POE chains and its frustration. In the core of the micelles, POE chains should be stressed, and hence, they experience frustration. The longer the chain, the greater is the chain frustration. Therefore, the long POE chains prefer to be in a shortened and laterally expanded structure. The expanded a_P, therefore, prefers less negative interfacial curvature. Figure 12b represents the variation of d, R, r_H, d_H, and a_P in the I_2, H_2, and L_α phases at 53 °C. d and a_P increase with the increase of n irrespective of the types of aggregates. The chain frustration can largely be reduced by the phase transitions from negative to zero interfacial curvature: I_2 to H_2 to L_α according to the decreasing tendency observed for the radius or the half-thickness of the polar domains. Within the same phase (I_2 or H_2), the radius, R or r_H, increases with n, whereas within the phase transitions (I_2-H_2 or H_2-L_α) there are step decreases of the radius or half-thickness of the poly(oxyethylene) domain: R to r_H to d_H.

$Si_mC_3EO_{51.6}$ System. Figure 13a represents the variation of d, r_H, d_H, d_L(half-thickness of the apolar layer in the L_α phase), r_L (half of the longest distance between polar cores of two cylinders), and a_P in the L_α

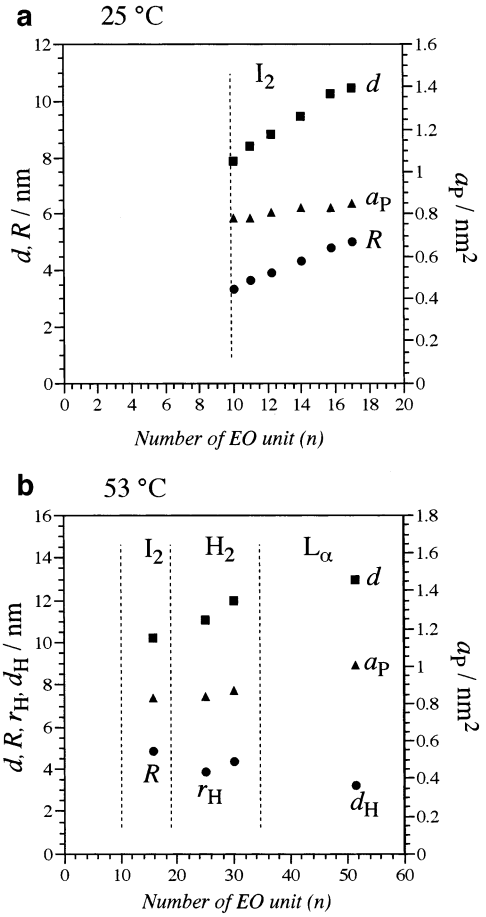

Figure 12. Structural parameters for the $Si_{25}C_3EO_n$ system as a function of n: (a) variation of d, R, and a_P in the I_2 phase at 25 °C; (b) variation of d, R, r_H, d_H, and a_P in the I_2, H_2 and L_α phases at 53 °C. Key: d (■), interlayer spacing; R, r_H, or d_H (●), radius of the polar (polyoxyethylene) core of micelles, cylinders, or half-thickness of the polar layer, respectively; a_P (▲), effective cross-sectional area per copolymer molecule.

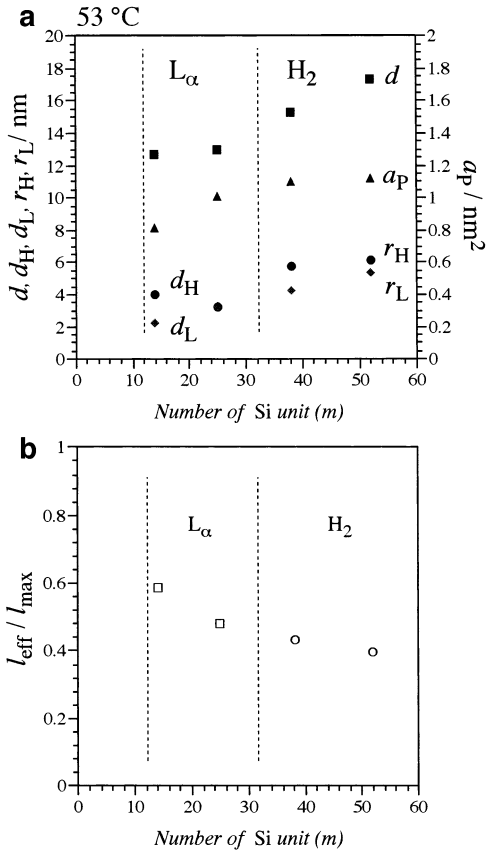

Figure 13. Variation of (a) d, d_H, d_L, r_H, r_L and a_P and (b) l_{efff}/l_{max} in the L_α and H_2 phases for the $Si_mC_3EO_{51.6}$ system, as a function of m at 53 °C. Key: d (■), interlayer spacing; d_H or r_H (●), half-thickness of the polar layer or radius of the polar core of cylinder; d_L or r_L (◆), half-thickness of the apolar layer or the half longest distance between polar cores of two cylinders corresponding to l_{eff}; a_P (▲), effective cross-sectional area per copolymer molecule. l_{max} is the extended chain length of the poly(dimethylsiloxane) part of the copolymer.

and H_2 phases as a function of the silicone chain length, m, at 53 °C. In the L_α phase, d_H (polar half-thickness) decreases a little bit and d_L (apolar half-thickness) increases; therefore, d ($= 2d_H + 2d_L$) slightly increases with the increase of m. a_P increases from 0.82 to 1.01 with the increase of m from 14 to 25. Since the poly(dimethylsiloxane) chain is very flexible, with the increase of its chain length the lateral pressure increases making the copolymer layer curvature more negative and expanding a_P. In our previous paper,[17] we have shown that there is an effect of the apolar chain length on the interfacial area. With the increase of the apolar length (m) the interfacial area increases and the copolymer layer curvature changes toward more negative.[17] In the present system, with the increase of m, a_P increases and the bilayer (L_α phase) changes to cylinders (H_2 phase) in which the silicone chain forms the corona of the cylinder. Hence, it has more space to distribute. In the H_2 phase, d and a_P increase, as a general trend, with m as described above, whereas r_H remains almost constant since the POE chain is constant. Although the POE chain is constant, when the L_α phase is changed to the H_2 phase the POE chain is stressed (because of the packing restriction) as can be deduced from the large difference between d_H and r_H. On the other hand, d_L and r_L, which can be also associated with the effective apolar length (l_{eff}) in the L_α and H_2 phases, respectively, increase continuously with m. However, l_{eff}/l_{max} decreases with increasing m as shown in Figure 13b, where l_{max} is the fully extended length of the PDMS chain. It reveals that a long polymer chain has a short laterally expanded structure compared with a short polymer chain, because the entropy loss is very large when a long chain is in its extended form. Therefore, a_P increases (Figure 13a) and at a certain m the L_α to H_2 phase transition occurs.

IV. Discussion

POE—PDMS M_w/T ($\sim\chi N$) vs f Phase Diagram. The phase behavior of one-component A−B block copolymer systems is often described in terms of the χN vs f phase diagram, where the product χN is a measure of the block segregation and controls the stability of the different ordered morphologies. f is the volume fraction of one block of the copolymer and primarily controls the shape and packing symmetry of the morphologies. For a further discussion we have constructed a "phase diagram" as a function of M_w/T vs f for the POE−PDMS system using transition temperatures shown in Figures 1 and 3 and have represented this phase diagram in Figure 14 in a way comparable to the χN vs f phase diagram used in copolymer melts. The ordered morphologies range from $f = 0.17$ to 0.69, in which $0.17 \le f \le 0.27$ corresponds to the I_2 phase, $0.27 \le f \le 0.39$ to the H_2 phase, and $0.4 \le f \le 0.69$ to the L_α phase. The ranges of f values where the different phases occur in

Table 2. Ranges of *f* Values for Each Phase in $Si_{25}C_3EO_n$, $Si_mC_3EO_{51.6}$, PI−PS Melts, and $Si_{25}C_3EO_n$−Water or $Si_{25}C_3EO_n$−D_4 Systems

	$Si_{25}C_3EO_n$				
copolymer phase	*f* in melt	*f* in water	*f* in D_4	$Si_mC_3EO_{51.6}$ *f* in melt	PI−PS[a] *f* in melt
O_m	0−0.17	0−0.09	0−0.16	*c*	0−0.20[b]
I_2	0.17−0.27	0.09−0.24	0.16−0.27	*c*	*d*
H_2	0.27−0.39	0.24−0.39	0.27−0.39	0.33−0.44	0.20−0.33
L_α	0.40−0.50	0.39−0.50	0.40−0.50	0.44−0.69	0.33−0.60

[a] Reference 7. [b] Disordered phase. [c] Not measured. [d] Not found.

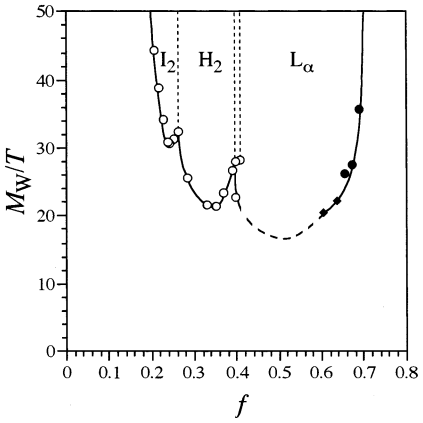

Figure 14. M_w/T ($\sim\chi N$) vs *f* phase diagram for $Si_mC_3EO_n$ copolymers. Open and filled circles correspond to the transition temperatures obtained from Figures 1 and 3, respectively. Filled diamonds (◆) correspond to the lamellar-disorder transition temperatures 149 and 155 °C for $Si_{14}C_3EO_{45}$ and $Si_{14}C_3EO_{51.6}$, respectively.

$Si_{25}C_3EO_n$, $Si_mC_3EO_{51.6}$ and polyisoprene−polystyrene (PI−PS)[7] melt systems, as well as in $Si_{25}C_3EO_n$−water and $Si_{25}C_3EO_n$−D_4 (octamethylcyclotetrasiloxane) lyotropic systems,[19] are shown in Table 2. Ordered microstructures start to form in the $Si_{25}C_3EO_n$−water system at lower *f* values ($f = 0.09$) than in the melt system ($f = 0.17$). The I_2−H_2 and H_2−L_α phase transitions occur in the copolymer/water binary system at lower *f* values than those observed in the corresponding copolymer melt system, indicating that the POE hydration increases the effective volume fraction of the POE block. It also is expected to enhance the segregation tendency[39] between POE and PDMS at lower temperature, where hydrogen bonds stiffen and cross-link the POE chains. Consequently, under hydrous conditions, the ordered structures can be formed at lower M_w of the copolymer.

The phase transition *f* values or the ranges of *f* values for different microstructures show almost no variation in the $Si_{25}C_3EO_n$ melt system compared with the $Si_{25}C_3EO_n$−D_4 system. Addition of silicone oil primarily does not cause additional segregation since the system already has the same characteristic poly(dimethylsiloxane), however it increases the overall effective apolar volume fraction and the interfacial flexibility. Hence the result is similar to the effect of increasing the PDMS chain in the copolymer;[18] that is, the copolymer layer curvature changes toward more negative values.[19] For example, a silicone copolymer with $f = 0.5$ forms the L_α phase in the melt, but L_α−H_2−I_2−O_m phase transitions take place with the addition of silicone oil.

Comparing with other copolymer melt systems, $Si_mC_3EO_n$ forms ordered morphologies at relatively low molecular weight. For example, in the PI−PS melt system, the sample with the lowest $M_n = 17\,000$, IS-54, forms lamellar liquid crystals below 124 °C.[7,40] $Si_{14}C_3EO_{12}$ ($M_w \approx 1600$, $N = 26$) and $Si_{25}C_3EO_{12.2}$ ($M_w \approx 2400$, $N = 37$) melts form H_2 and I_2 phases,[18] respectively, although the molecular weights of these silicone copolymers are about 10 times lower than that of the PI−PS melt. For many monomer pairs the interaction parameter χ is $\sim$ 0.1, so the micro phase separation should not occur for chains $N < 100$, since for $\chi N < 10$ only a disordered phase is stable.[5] A study of the PDMS−POE−PDMS triblock system reveals that χ for POE−PDMS is $\sim$ 0.4−1.1, with the higher limit corresponding to high POE volume fractions in the copolymer.[20] A large value of the interaction parameter has also been recently reported by Ren et al. for fluorinated diblock copolymers.[41] Even if we consider the χ parameter for the present POE−PDMS diblock copolymer to be only 0.4, the copolymer will undergo microphase separation at $\sim N = 25$; a value which is consistent with the observed results.

The POE−PDMS one-component system shows differences from other theoretically predicted or experimentally studied phase diagrams. This might be due to the unusual incompatibility of PDMS and POE chains even in the low molecular weight range. The system already forms POE-core micelles in the vicinity of the ordered cubic structure. The observed I_2 phase belongs to a $Fd\bar{3}m$ space group, which is uncommon in the copolymer melt systems and has not yet been predicted by the theoretical models that only account for the existence of the most commonly found bcc phase, although, a normal fcc lattice (close-packed, thus Q^{225} and alternatively hcp) has been already assumed by Matsen et al.[32] We did not observe the intermediate bicontinuous cubic (V_1 or V_2) and HPL (perforated layers) phases in our system, probably because of the rigidity of the POE−PDMS interface. Mixing the copolymers with low molecular weight surfactants (e.g., $Si_{25}C_3EO_{51.6}$ + $C_{12}EO_5$) increases the flexibility of the polar−apolar interface, and hence, the mixtures form the V_2 phase in water.[42] $Si_mC_3EO_n$ melts form the L_α phase in the range $0.4 \le f \le 0.69$, and no normal (PDMS core and POE corona) morphologies are observed for $f > 0.69$, whereas the PI−PS system forms the hexagonal phase at this *f* value. However, normal hexagonal (H_1) and cubic (I_1) phases are observed in the $Si_{5.8}C_3EO_{51.6}$($f = 0.8$)−water binary system.[43]

The asymmetric phase diagram (Figure 14) can be interpreted in terms of a conformational asymmetry parameter, $\epsilon = \beta_A^2/\beta_B^2$, where $\beta^2 = R_g^2/V = a^2/6v$, with the parameter notations taken from ref 8. ϵ accounts for differences in the conformational and volume-filling characteristics of blocks and being $\epsilon \neq 1$ produces of an asymmetric phase diagram. For a compositionally symmetric silicone copolymer ($f = {}^1/_2$), $Si_{25}C_3EO_{51.6}$, $\epsilon = \beta_{POE}^2/\beta_{PDMS}^2 \approx 2.8$ indicates the large difference in space-filling characteristics between the POE and PDMS.

In the $Si_mC_3EO_n$ melt system, when the PDMS chain is very short, the segregation tendency is obviously not strong enough to induce microphase separation. Packing the more flexible PDMS block in the core of a copolymer micelle requires strong swelling of the polar side of the interface, either by cosurfactants or by water. Therefore, the lamellar phase is observed in a wide range of f values in the melt. The observed asymmetric phase behavior of the POE−PDMS copolymer melt can be ascribed to the fact that the block, which is stericaly more voluminous at the interface, due to its higher cross-section, has the highest flexibility and lowest cohesive energy. It seems that it is advantageous to have the softer block in the periphery of the primary self-assembled structures, especially when the structures need to fill the space as effective as possible. Also, in a nucleation and growth (NG) segregation process the self-assembly of the blocks with the higher cohesive energy to form the cores is favored.

V. Conclusion

Poly(oxyethylene)−poly(dimethylsiloxane) diblock copolymer melts form different ordered morphologies: micellar cubic, hexagonal and lamellar phases even at a comparatively low molecular weight because of the incompatibility of POE and PDMS blocks. The lamellar phase extends up to high f values, and (PDMS in POE) micelles, assembled into the most common hexagonal or cubic (bcc Q,[229] fcc Q[225]) phases have not been found in this melt system. Instead, the observed cubic phase assembled with POE in PDMS micelles seems to belong to the $Fd\bar{3}m$ space group, which has not been found, until now, in other copolymer melt systems, the bcc structure being the favored one. The reason for that may lie in the high flexibility of the PDMS block which allows the formation of a more packed structure without much frustration, as happens in copolymer−solvent mixtures. The calculated asymmetry parameter for the compositional symmetric copolymer ($Si_{25}C_3EO_{51.6}$) clearly indicates that the space-filling characteristics of the PDMS block is very large compared with the POE and agrees with the previous interpretation. However, at this stage we do not have a clear argument to interpret the existence of this $Fd\bar{3}m$ structure, and other reasons, such as the influence of the polydispersity of our samples, cannot be ruled out.

The flexibility and low cohesive energy of long PDMS chains allow them to form soft, almost liquidlike coronae, whereas the higher cohesive energy of the POE chains favors their self-assembly into the micellar cores, which tend to become crystalline at much higher temperatures than would tend to be observed for the PDMS.

Acknowledgment. We thank Asao Harashima and Haruhiko Furukawa at Dow Corning Toray Silicone Co. Ltd., Japan, for supplying us the silicone copolymers. Professor Dr. Tadashi Kato (Tokyo Metropolitan University) is acknowledged for help with the synchrotron radiation SAXS experiment.

References and Notes

(1) Bates, F. S.; Fredrickson, G. H. *Annu. Rev. Phys. Chem.* **1990**, *41*, 525−557.
(2) Matsen, M.; Schick, M. *Curr. Opin. Colloid Interface Sci.* **1996**, *1*, 329.
(3) Lohse, D. J.; Hadjichistidis, N. *Curr. Opin. Colloid Interface Sci.* **1997**, *2*, 171−176.
(4) Aggarwal, S., Ed. *Block Copolymers*; Plenum Press; New York, 1970.
(5) Leibler, L. *Macromolecules* **1980**, *13*, 1602−1617.
(6) Matsen, M.; Bates, F. S. *J. Chem. Phys.* **1997**, *106*, 2436−2448.
(7) Khandpur, A. K.; Forster, S.; Bates, F. S.; Hamley, I. W.; Ryan, A. J.; Bras, W.; Almdal, K.; Mortensen, K. *Macromolecules* **1995**, *28*, 8796−8806.
(8) Bates, F. S.; Schulz, M. F.; Khandpur, A. K.; Forster, S.; Rosedale, J. H.; Almdal, K.; Mortensen, K. *Faraday Discuss. Chem. Soc.* **1994**, *98*, 7−18.
(9) Huang, K.-L.; Shigeta, K.; Kunieda, H. *Prog. Colloid Polym. Sci.* **1998**, *110*, 171−174.
(10) Kunieda, H.; Shigeta, K.; Ozawa, K.; Suzuki, M. *J. Phys. Chem. B* **1997**, *101*, 7952−7957.
(11) Uddin, Md. H.; Kanei, N.; Kunieda, H. *Langmuir* **2000**, *16*, 6891−6897.
(12) Hillmyer, M. A.; Bates, F. S.; Almdal, K.; Mortensen, K.; Ryan, A. J.; Fairclough, J. P. A. *Science* **1996**, *271*, 976−978.
(13) Hajduk, D. A.; Kossuth, M. B.; Hillmyer, M. A.; Bates, F. S. *J. Phys. Chem. B* **1998**, *102*, 4269−4276.
(14) Mai, S.-M.; Fairclough, J. P. A.; Hamley, I. W.; Matsen, M. W.; Denny, R. C.; Liao, B.-X.; Booth, C.; Ryan, A. J. *Macromolecules* **1996**, *29*, 6212−6221.
(15) Alexandridis, P. *Curr. Opin. Colloid Interface Sci.* **1997**, *2*, 478−489.
(16) *Silicone Surfactants*; Hill, R. M., Ed.; Surfactant Science Series 86; Marcel Dekker: New York, 1999.
(17) Kunieda, H.; Uddin, Md. H.; Horii, M.; Furukawa, H.; Harashima, A. *J. Phys. Chem. B* **2001**, *105*, 5419−5426.
(18) Rodriguez, C.; Uddin, Md. H.; Watanabe, K.; Furukawa, H.; Harashima, A.; Kunieda, H. *J. Phys. Chem. B* **2002**, *106*, 22−29.
(19) Uddin, Md. H.; Yamashita, Y.; Furukawa, H.; Harashima, A.; Kunieda, H. *Prog. Colloid Polym. Sci.*, in press.
(20) Galin, M.; Mathis, A. *Macromolecules* **1981**, *14*, 677−683.
(21) Almdal, K.; Mortensen, K.; Ryan, A. J.; Bates, F. S. *Macromolecules* **1996**, *29*, 5940−5947.
(22) Uddin, Md. H.; Rodriguez, C.; Watanabe, K.; López-Quintela, A.; Kato, T.; Furukawa, H.; Harashima, A.; Kunieda, H. *Langmuir* **2001**, *17*, 5169−5175.
(23) Seddon, J. M. *Biochemistry* **1990**, *29*, 7997−8002.
(24) Alexandridis, P.; Olsson, U.; Lindman, B. *Langmuir* **1996**, *12*, 1419−1422.
(25) Singh, M. A.; Ghosh, S. S.; Shannon Jnr., R. F. *J. Appl. Crystallogr.* **1993,** *26*, 787−794.
(26) Mendelkern, L. In *Crystallization of polymers*; McGraw Hill: New York, 1964; Chapter 2, p 33.
(27) Mortensen, K. *Polym. Adv. Technol.* **2001**, *12*, 2−22.
(28) McQuarrie, D. A. In *Statistical Thermodynamics*; Harper & Row: New York, 1976; Chapter 13.
(29) Mariani, P.; Luzzati, V.; Delacroix, H. *J. Mol. Biol.* **1988**, *204*, 165−189.
(30) Charvolin, J.; Sadoc, J. F. *J. Phys. (Paris)* **1988**, *49*, 521−526.
(31) Luzzati, V.; Vargas, R.; Gulik, A.; Mariani, P.; Seddon, J. M.; Rivas, E. *Biochemistry* **1992**, *31*, 279−285.
(32) Matsen, M. W. *Phys. Rev. Lett.* **1995**, *74*, 4225−4228.
(33) Mariani, P.; Rivas, E.; Luzzati, V.; Delacroix, H. *Biochemistry* **1990**, *29*, 6799−6810.
(34) Pedersen, J. S. *Adv. Colloid Interface Sci.* **1997**, *70*, 171−210.
(35) Pedersen, J. S.; Gerstenberg, M. C. *Macromolecules* **1996**, *29*, 1363−1365.
(36) Ganazzoli, F.; Allegra, G.; Higgins, J. S.; Roots, J.; Bruckner, S.; Lucchelli, E. *Macromolecules* **1985**, *18*, 435−442.
(37) Baxter, R. J. *J. Chem. Phys.* **1968**, *49*, 2770−2774.
(38) Watzlawek, M.; Likos, C. N.; Löwen, H. *Phys. Rev. Lett.* **1999**, *82*, 5289−5292.
(39) Kunieda, H.; Shinoda, K. *J. Dispersion Sci. Technol.* **1982**, *3*, 233−244.
(40) Gehlsen, M. D. Ph.D. Thesis, University of Minnesota, 1994.
(41) Ren, Y.; Lodge, T. P.; Hillmyer, M. A. *Macromolecules* **2002**, *35*, 3889−3894.
(42) Kunieda, H.; Uddin, Md. H.; Furukawa, H.; Harashima, A. *Macromolecules* **2001**, *34*, 9093−9099.
(43) Rodriguez, C.; Uddin, Md. H.; Furukawa, H.; Harashima, A.; Kunieda, H. *Prog. Colloid Polym. Sci.* **2001**, *118*, 53−56.

MA0210978